# Vertical distribution of gravity wave potential energy from long-term Rayleigh lidar data at a northern middle-latitude site

Nahoudha Mzé, Alain Hauchecorne, Philippe Keckhut, Michèle Thétis

AGU PUBLICATIONS

JGR

Journal of Geophysical Research: Atmospheres

RESEARCH ARTICLE
10.1002/2014JD022035

**Key Point:**
- We give an overview of the gravity wave activity using Rayleigh lidar

**Correspondence to:**
N. Mzé,
nahoudha.mze@latmos.ipsl.fr

**Citation:**
Mzé, N., A. Hauchecorne, P. Keckhut, and M. Thétis (2014), Vertical distribution of gravity wave potential energy from long-term Rayleigh lidar data at a northern middle-latitude site, *J. Geophys. Res. Atmos.*, *119*, 12,069–12,083, doi:10.1002/2014JD022035.

Received 15 MAY 2014
Accepted 10 OCT 2014
Accepted article online 14 OCT 2014
Published online 13 NOV 2014

# Vertical distribution of gravity wave potential energy from long-term Rayleigh lidar data at a northern middle-latitude site

**N. Mzé[1], A. Hauchecorne[1], P. Keckhut[1], and M. Thétis[1]**

[1]LATMOS-IPSL, Université Versailles St-Quentin, Sorbonne Universités, UPMC Université Paris 6, CNRS/INSU, Guyancourt, France

**Abstract** In this paper, we use the Rayleigh lidar in order to give an overview of the gravity wave activity at a northern middle-latitude station at Haute-Provence Observatory (43.93°N, 5.71°E). In order to have access to perturbations with short time and vertical scales, at least in a statistical sense, we analyze raw lidar signals with a variance method. Sixteen years of lidar data sets are analyzed in this study. The results of the variability, climatology, and seasonal changes are reported. We observe night-to-night variability in gravity wave potential energy, which follows a lognormal distribution with a standard deviation ranging between 0.50 and 0.58 (base 10 logarithm). A monthly distribution of gravity waves is also obtained in the upper stratosphere and mesosphere. In the 30–50 km altitude range (the upper stratosphere), an annual cycle is clearly found with a maximum in winter and a minimum in summer. An annual cycle in the lower mesosphere is also observed with maximum in winter. In the upper mesosphere, a semiannual cycle is found at ~75 km. At this altitude, the maximum gravity wave activity occurs in winter and in summer. A more pronounced summer maximum is observed (+25%). The summer maximum at Haute-Provence Observatory in the upper mesosphere is probably due to oblique propagation. Looking at the seasonally averaged profiles, it is possible to observe the preferential altitudes of energy dissipation. Gravity waves are dissipating above ~70 km during all seasons, but there is relatively little dissipation at lower altitudes.

## 1. Introduction

Gravity waves are known to play a major role in the energy and momentum budget in the middle atmosphere and thereby to influence the atmospheric structure and circulation [*Lindzen*, 1981; *Fritts and Alexander*, 2003; *Alexander et al*., 2010]. In fact, there is a multitude of gravity wave sources such as deep convection, topography, wind shears, jet streams, and wave-wave interactions [e.g., *Fritts and Alexander*, 2003, and references therein]. In numerical weather prediction and climate simulation models, however, only very simplified gravity wave drag parameterizations are used [*Kim et al*., 2003]. A recent comparison of such parameterizations and observations [*Geller et al*., 2013] reveals larger differences but also shows that additional data are required for constraining the gravity wave parameterization schemes. Thus, observational studies are needed to describe the climatology of gravity waves in the middle atmosphere and in order to improve parameterizations in models.

More observational information is needed in the altitude ranges where interactions of the gravity waves and the mean flow occur (i.e., where gravity wave energy dissipates). Climate models require to include a drag effect of these waves and to validate with observations [*Kim et al*., 2003]. Even models with adequate spatial resolutions and a direct representation of gravity waves need an evaluation of the resulting drag. It is possible to derive from Rayleigh lidar profiles highly, vertically resolved dynamical quantities associated with the propagation of gravity waves. The vertical evolution of such quantities can then provide very useful information on the altitude regions where these gravity waves dissipate. It shoud be noted that if a wave (or even in average a multitude of waves) is propagating, e.g., from low to high latitudes, this wave may be at the position of the lidar only in a limited altitude range (oblique propagation).

Different satellites and ground-based techniques (lidar, radar, radiosonde, rocket sounding, and airglow imagers) have provided information about the gravity wave activity. The lidar technique allows observations from the troposphere up to the lower thermosphere, and it gives access to vertical profiles of atmospheric parameters and to their temporal evolution. In particular, Rayleigh lidar provides vertical profiles of the total density of the atmosphere from about 30 km to 90 km depending on the signal-to-noise ratio [*Hauchecorne and Chanin*, 1980]. Thus, it is a powerful tool for the study of atmospheric perturbations. Preliminary results have

shown that lidar instruments produce accurate observations with high temporal and spatial resolution, well adapted for studying atmospheric gravity waves [*Chanin and Hauchecorne*, 1981; *Shibata et al*., 1986; *Gardner and Voelz*, 1987]. Following this, gravity wave activity has been extensively analyzed using lidars throughout the middle atmosphere in several studies at low-latitude stations [*Beatty et al*., 1992; *Chane-Ming et al*., 2000; *Sivakumar et al*., 2006; *Li et al*., 2010], at midlatitude sites [*Gardner et al*., 1989; *McDonald et al*., 1998; *Mitchell et al*., 1991; *Murayama et al*., 1994; *Rauthe et al*., 2006, 2008; *Senft and Gardner*, 1991; *Sica and Argall*, 2007; *Whiteway and Carswell*, 1995], at high-latitude sites, and over the Poles [*Alexander et al*., 2011; *Blum et al*., 2004; *Collins et al*., 1994; *Duck et al*., 2001; *Yamashita et al*., 2009; *Whiteway et al*., 1997]. Gravity wave spectra, climatology, and variability were already investigated in the south of France using Rayleigh lidar [*Wilson et al*., 1990, 1991a, 1991b; *Hauchecorne et al*., 1994].

All these studies reveal temperature and density anomalies growing with altitude as a result of density decreasing with heights. Dissipation should be present at all heights but be particularly enhanced at vertical wind gradients and where gravity waves break. Mesospheric inversions observed frequently on temperature profiles [*Hauchecorne et al*., 1987; *Meriwether and Gardner*, 2000] were interpreted as the result of such interactions [*Hauchecorne and Maillard*, 1990].

These lidar investigations in the midlatitude studies revealed an annual cycle in the upper stratosphere and a semiannual variation in the upper mesosphere. In particular, *Wilson et al*. [1991b] found that the maximum of wave activity occurs during winter and a minimum during summer in the stratosphere and lower mesosphere over two sites in France: Haute-Provence Observatory (43.93°N, 5.71°E) and Biscarosse (44°N, 1°W). A semiannual component is reported and superimposed on the annual cycle above 60 km with a secondary maximum in summer.

Rayleigh lidar provides vertical profiles of molecular density and temperature when the atmosphere is free of aerosols (Rayleigh scattering above 30 km). In order to obtain a signal-to-noise ratio sufficiently large to detect atmospheric perturbations, it is necessary to sum the raw lidar signals in time and vertically before doing the data processing, which limits the achievable vertical and temporal resolutions of such measurements. Due to the signal-to-noise ratio of the measurements, which increases with integration time and vertical smoothing, it is only possible to detect perturbations with periods and vertical wavelengths large enough to be above the noise. In order to have access to perturbations with shorter time and vertical scales, at least in a statistical sense, we analyze lidar signals with a variance method. This method is based on the computation of the signal perturbations over short time and vertical intervals and on the summation of the square of these perturbations over a large number of elementary intervals, which give an estimation of their variance. It allows extracting the root-mean-square mean amplitude of small-scale perturbations that are not detectable on single profiles. Therefore, the variance method has been applied in the estimation of the gravity wave energy in the upper stratosphere and in the mesosphere. It is a simple and robust way to estimate the potential energy per unit mass of gravity waves in large spectral bands, and it is useful for both climatological or case studies [*Hauchecorne et al*., 1994]. The mean stratopause altitude does not vary much during the year at Haute-Provence Observatory. The mean altitude for stratopause and mesopause is 47 km and 86 km, respectively [*Hauchecorne et al*., 1991].

The objective of this study is the quantification of gravity wave energy lost as a function of altitude based on lidar signal analysis. In this manuscript, we present an estimation of the gravity wave activity in the middle atmosphere over a lidar station located at Haute-Provence Observatory (hereafter OHP) by the use of a robust method, easy and rapid to implement on large lidar databases. This study investigates 16 years of measurements (from January 1996 to December 2012). The paper is organized as follows: Section 2 presents the data measurements and describes the variance method. Section 3 presents the application to a Rayleigh lidar signal. In section 4, the entire data set is analyzed, and the results of the variability and an average annual cycle are reported. Section 5 describes the seasonal changes of gravity wave energy and dissipation. In section 6, we compare the results with previous studies in midlatitude stations, and the results are discussed. Section 7 concludes the results.

## 2. Data Set and Variance Method

### 2.1. Lidar Measurements and Analysis Technique

Lidar measurements [*Hauchecorne and Chanin*, 1980] over OHP in the middle atmosphere have been intensively used for dynamical studies [*Wilson et al*., 1990; *Hauchecorne et al*., 2009], for satellite validation

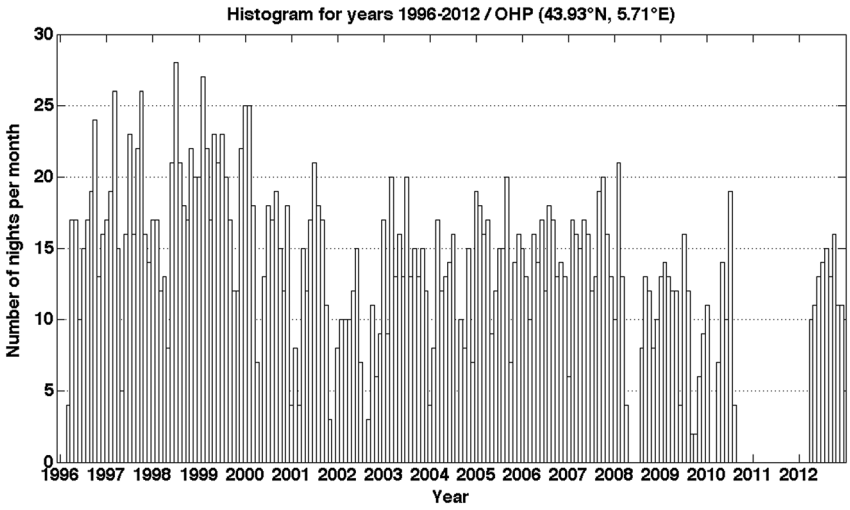


**Figure 1.** Monthly distributions of the number of nights measured from the Rayleigh lidar over OHP (43.93°N, 5.71°E) for the period 1996 to 2012.

[*Ridolfi et al*., 2007; *Sica et al*., 2008], and within the NDACC (Network for the Detection of Atmospheric Composition Changes) for trend detection, where intercomparisons with a mobile instrument [*Singh et al*., 1996] were conducted showing an accuracy better than 1 K up to 70 km. Multidecadal series were obtained, and this has allowed the detection of middle atmosphere cooling due to ozone decrease and greenhouse gas increase [*Steinbrecht et al*., 2009].

The lidar technique is based on a pulsed laser sent vertically. The light echo is detected with a telescope at ground collecting photons being backscattered by either atmospheric molecules or particles. This method is very efficient for detecting aerosol and cloud vertical structures. In the absence of aerosols, the molecular scattering can be used to derive atmospheric density or temperature profiles [*Hauchecorne et al*., 1992] from 30 to 80–90 km. The first altitude corresponds to the limit where atmosphere can be considered as free of aerosol scattering, and the top altitude corresponds to the altitude where backscattering light is masked by the noise due either to intrinsic photomultiplier noise ($<$100 c/s) or background light. The background light is reduced considerably during nighttime operations and by the use of narrow telescope field of view (0.3 mrad) and narrow band-pass filter (10 nm) to select only the laser light.

Systematic errors can occur and are strongly related to the lidar design as well as the tuning. Potential errors have been listed by *Keckhut et al*. [1993] and concern mainly the alignment between laser and telescope, linearity of the detection, and noise estimates. In addition to such instrument limitations, a general main uncertainty is the counting statistics associated with the number of photons and the background noise ($B$) with the following relation:

$$\frac{\Delta\rho(z)}{\rho(z)} = \frac{\sqrt{n(z)+B}}{n(z)} \quad (1)$$

With $\rho(z)$ and $n(z)$ being, respectively, the atmospheric density and the number of backscatter photons collected as a function of altitude. Improving the accuracy requires an increase in the number of photons. This can be achieved by using powerful laser with high repetition rate and a large area telescope. The lidar is composed of a frequency-doubled Nd:Yag laser emitting at 532 nm with a repetition rate of 50 Hz and a collector surface area composed of a mosaic of four mirrors with a diameter of 50 cm corresponding to a surface of 0.8 $m^2$. More details are given by *Keckhut et al*. [1993].

Lidar measurements are performed continuously at OHP since late 1978. In the beginning, the vertical resolution was 0.3 km, and it has been improved to 0.075 km since the mid-1990s. Figure 1 displays the monthly numbers of nighttime profiles derived from Rayleigh lidar at OHP from January 1996 to December 2012. We only focus on the period January 1996 to December 2012 because the acquisition system has been changed in mid-2013 with a new data format not taken into account by our data processing software. We only used nighttime profiles. As stated earlier, during nighttime, the background noise decreases

considerably. It should be noted that there is no lidar data in 2011 due to technical problems. The number of observations used in this work is 2079 profiles covering 16 years, and we discarded 30 profiles because they present aberrant points.

### 2.2. Variance Method

The variance method is relatively simple but has the advantage of being fast and using raw data. Thus, it is independent of data processing errors [*Hauchecorne et al*., 1994]. During the international campaign Dynamics Adapted Network for the Atmosphere, based on the study of the gravity wave activity and its relation with prevailing winds, *Hauchecorne et al*. [1994] found, except for a few nights, a very satisfactory agreement (correlation coefficient of 0.62 in the 30–45 km layer and 0.79 in the 40–55 km layer) between this method and a more sophisticated spectral method at Biscarrosse (44°N, 1°W) from January to March 1990. In this spectral method, the gravity wave energy is integrated in the vertical wavelength range from 1 to 10 km, and measurement noise is assumed to be white and estimated by a statistical method (for more details, see *Wilson et al*. [1991a]).

We consider the signal of an incoherent backscatter lidar operated in photon-counting mode. This raw signal is summed up in small time-vertical elementary intervals ($\Delta t$, $\Delta z$). We assume that the vertical profile of the signal may be separated in a sum of a smooth mean profile plus short-scale perturbations ($S = \overline{S} + dS$), with the amplitude much smaller than the mean profile. The relative perturbation ($S'$) is defines as

$$S'(z_i, t_j) = \frac{dS}{\overline{S}} = \frac{S(z_i, t_j) - \frac{1}{2}\left[S(z_{i-1}, t_j) + S(z_{i+1}, t_j)\right]}{\frac{1}{2}S(z_i, t_j) + \frac{1}{4}\left[S(z_{i-1}, t_j) + S(z_{i+1}, t_j)\right]} \tag{2}$$

where $S(z_i, t_j)$ and $S'(z_i, t_j)$ are the signal and perturbation at altitude $z_i$ and time $t_j$ in raw counts. Perturbations are due either to instrumental noise or atmospheric perturbations.

We consider now a larger time-vertical interval ($\Delta T$, $\Delta Z$) obtained by grouping $N_t$ elementary time intervals by $N_z$ elementary altitude intervals such as $\Delta T = \Delta t N_t$ and $\Delta Z = \Delta z N_z$. The observed variance of the signal in the large interval is defined as

$$V_{\text{obs}} = \frac{1}{N_z N_t} \sum_{N_z} \sum_{N_t} S'(z_i, t_j)^2 \tag{3}$$

The variance is the sum of instrumental and atmospheric variances. In the photon-counting mode, the signal obeys the Poisson's law, and accordingly, the instrumental variance can easily be calculated from the estimated mean signal $S$, except for saturation effects in case of exceptional strong signals:

$$V_{\text{inst}} = \frac{1}{N_z N_t} \sum_{N_z} \sum_{N_t} \frac{S(z_i, t_j) + \frac{1}{4}\left[S(z_{i-1}, t_j) + S(z_{i+1}, t_j)\right]}{\left\{\frac{1}{2}S(z_i, t_j) + \frac{1}{4}\left[S(z_{i-1}, t_j) + S(z_{i+1}, t_j)\right]\right\}^2} \tag{4}$$

The estimation of the atmospheric variance is obtained by the difference

$$V_{\text{atm}} = V_{\text{obs}} - V_{\text{inst}} \tag{5}$$

Then, the atmospheric variance will provide an estimation of the gravity wave activity in the middle atmosphere. The method is computed to study small-scale vertical perturbations from 30 km to 85 km with different values of $N_t$ and $N_z$. More details about the method are given in Appendix A.

## 3. Application to Rayleigh Signal and Potential Energy Estimates

In the analysis presented above and in Appendix A, the mean signal was assumed to be constant with altitude. This is not the case for a Rayleigh lidar for which the mean signal is proportional to the atmospheric density divided by the square of the distance between the lidar and the studied layer [*Hauchecorne and Chanin*, 1980]. If we assume an isothermal atmosphere, the mean signal corrected for the distance dependence will follow the exponential decrease of the atmosphere:

$$\overline{S(z)} = S_0 e^{-\frac{z}{H}} \tag{6}$$

where $z$ is the altitude and $H$ is the scale height of the atmospheric density.

In the more general case of an ordinary temperature profile, the density profile can be locally fitted by an exponential decrease on which small-scale perturbations are superimposed. We have to change equation (2) in order to cancel the influence of the exponential decrease of the mean signal (equation (6)) in the estimation of the perturbation. The variance of the Rayleigh signal can be approximated by

$$S'(z_i,t_j)=\frac{S(z_i,t_j)-\sqrt{S(z_{i-1},t_j)*S(z_{i+1},t_j)}}{\frac{1}{2}\left[S(z_i,t_j)+\sqrt{S(z_{i-1},t_j)*S(z_{i+1},t_j)}\right]} \tag{7}$$

For small perturbations, the first-order linearization in $z$ of the terms under the square roots leads to equation (2), but an exponential decrease of $S$ as a function of $z$ gives, $S'=0$. All results demonstrated using the linear formula are still valid with the exponential formula. For application to atmospheric lidar data, the exponential formula will be used in this study.

The assumption that the mean density follows an exponential decrease is valid when we consider small-scale perturbations (small values of $\Delta Z$). If we want to estimate the variance of large-scale perturbations ($\Delta Z$ of a few kilometers), this assumption is no longer valid, and we have to fit the mean density by a more complex analytic function in order to extract the background density profile. The estimation of the three-point variance, defined in our study, with a given thickness $\Delta Z$ of the layers is equivalent to estimating the power spectral density of atmospheric fluctuations in the band-pass filter with characteristics related to $\Delta Z$. The central wavelength and the bandwidth of this filter are proportional to $\Delta Z$, the central wavelength being a priori in the order of $2\Delta Z$ [*Hauchecorne et al.*, 1994]. This method is equivalent to an estimation of the variance using a broad passband filter centered at a wavelength $\lambda \approx 2.4\Delta Z$ (the width of the passband at half amplitude is approximately $\Delta\lambda \approx \lambda$). More details about the spectral analysis are given in Appendix B.

We used the potential energy per unit mass, $E_p$ (in J kg$^{-1}$), in order to characterize gravity wave activity, and it is calculated using the equation [*Wilson et al.*, 1991a]:

$$E_p=\frac{1}{2}\left(\frac{g}{N}\right)^2 V_{\text{atm}} \tag{8}$$

where $g$ is the gravitational acceleration (~9.8 m s$^{-2}$), $N$ is the Brunt–Väisälä frequency, and $V_{\text{atm}}$ is the atmospheric variance. The variance method has been computed for each night of our study in the altitude range between 30 km and 85 km. It is then expressed in potential energy using the Brunt–Väisälä frequency from the mean lidar temperature profile. We used the median and the interquartile range as a robust estimator of the $E_p$ profile statistics. In this way, the study of gravity wave climatology is less affected by outliers, and we also remove intermittency.

Figure 2 illustrates an example of the variance technique described above, and we focus on the lidar signal recorded on 26 January 2007 over OHP. The total variance of the signal (red line) is computed (Figure 2a). The result is then compared to the theoretical variance due to instrumental noise in the absence of atmospheric perturbations (blue line), i.e., the random noise, assuming a Poisson's law for the statistics of the signal. In Figure 2b, the atmospheric variance is represented, and the horizontal error bars indicate the $\pm 2\sigma$ confidence interval. Figure 2c displays the height profile of potential energy per unit mass, $E_p$, associated with the gravity wave perturbations. The conservative growth curve, exp ($z$/$H$), is superimposed. The density scale height $H$ is approximately 7 km in the middle atmosphere [*Fritts and Alexander*, 2003]. For nondissipative linear gravity wave propagation, the induced temperature perturbations will grow with height, in response to diminishing density, proportionally to exp ($z$/2$H$). The potential energy per unit mass will increase as exp ($z$/$H$), while the energy per unit volume remains constant [*Wilson et al.*, 1991a; *Whiteway and Carswell*, 1995].

The three-point variance is computed with $N_t = 10$ and with $N_z = 20$ in the 30–50 km altitude range in the upper stratosphere and $N_z = 40$ above 50 km in the mesosphere. *Wilson et al.* [1990] reported that the mean vertical wavelength of the gravity waves increases with height from the lower stratosphere to the upper mesosphere. We expect that from saturation theory [e.g., *Warner and McIntyre*, 1999], and we can also find it in global data [*Ern et al.*, 2011]. Moreover, due to the decrease of the signal-to-noise ratio with height, it is not possible to detect the short-wavelength perturbations in the mesosphere [*Hauchecorne et al.*, 1994]. The choice of $N_z$ is a trade-off between several criteria: if you take too small values, the signal-to-noise ratio is too small to be detectable, and if you take too large values, you could include structures in the mean temperature

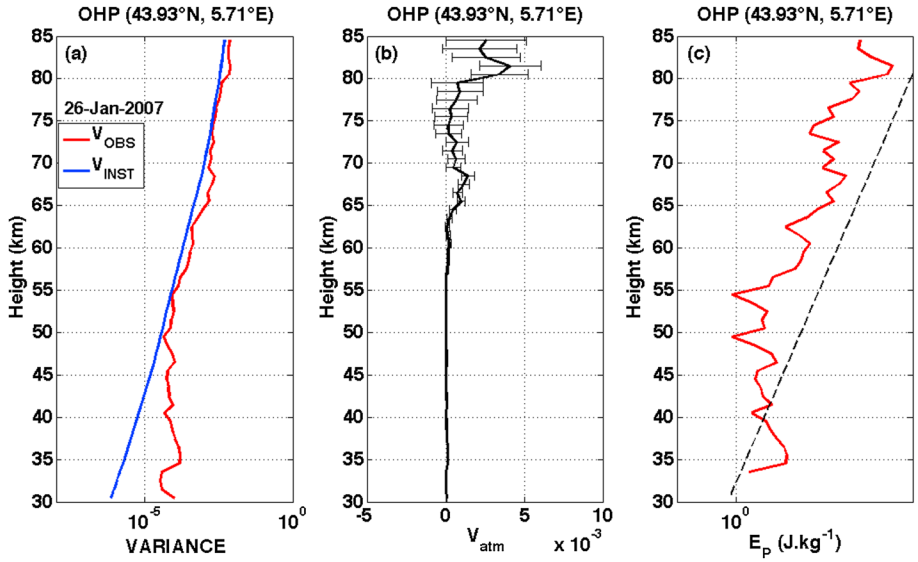


**Figure 2.** (a) Vertical profiles of observed (red line) and instrumental (blue line) variance as obtained from Rayleigh lidar over OHP (43.93°N, 5.71°E) on 26 January 2007. (b) Vertical profile of atmospheric variance. The horizontal error bars indicate the ±2σ confidence interval. (c) Gravity wave potential energy per unit mass (in $J.kg^{-1}$) in the upper stratosphere and mesosphere. The black dashed line refers to the adiabatic growth curve, exp ($z/H$); the density scale height $H$ is approximately 7 km in the middle atmosphere.

profile, which are not associated with gravity waves. The OHP lidar provides vertical profiles of raw signal with temporal and vertical resolutions of 2 min 40 s and 0.075 km, respectively. $N_z$ values (20 and 40) define the average wavelength selected by the band-pass vertical filter used in the variance method to study small-scale vertical perturbations (gravity waves). $N_z = 20$ corresponds to a band-pass filter centered at about 3.6 km and $N_z = 40$ at ~7.1 km (see also Appendix B and Figure B1). The lidar profiles have been integrated over ~26 min. The integration time used limits the shortest period which can be measured (~52 min).

## 4. Variability and Climatology of Gravity Wave Potential Energy

Histograms of the nightly distributions of the logarithm of potential energy per unit mass in the upper stratosphere and mesosphere derived from lidar observations are illustrated in Figure 3 at different altitudes. The distribution of the logarithm of potential energy is approximately Gaussian at all altitudes, indicating that it follows a lognormal distribution. There are a small number of values much lower than the average. This may be due to the larger relative uncertainty when the energy is very low. The width of the distribution is almost constant with altitude with a standard deviation ranging between 0.50 and 0.58 (base 10 logarithm, factor 3.1 to 3.8 in energy). The night-to-night variability of the gravity wave activity is also visible in the nightly mean $E_p$ time series (not shown).

Figure 4 displays the monthly distributions of potential energy per unit mass in the 30–50 km altitude range and between 50 km and 85 km, as computed from lidar measurements. $E_p$ is colored in a logarithmic scale (log10). Some clear seasonal variations emerged in the data in the upper stratosphere. We found an annual cycle with a maximum of gravity wave activity occurring in winter and a minimum in summer between 30 km and 50 km. Gravity wave activity increases systematically in winter months and decrease in summer months. An interannual variability is observed. The winter maximum magnitude of gravity wave activity changes from one year to another. It can be seen from the figure that there is some strong gravity wave activity in 2005. The winter maximum of gravity wave activity is more pronounced in 2004–2005, in comparison with other winters. We also report a decrease in gravity wave activity in the 2008–2009 winter maximum. In the lower mesosphere, an annual cycle is observed with maximum in winter and minimum during summer. In the upper altitudes, it appears difficult for the moment to detect some clear seasonal variation in the gravity wave activity, but we sometimes report a maximum of gravity wave activity in winter (e.g., 2001, 2005, and 2007) and in summer (e.g., 1999 and 2005).

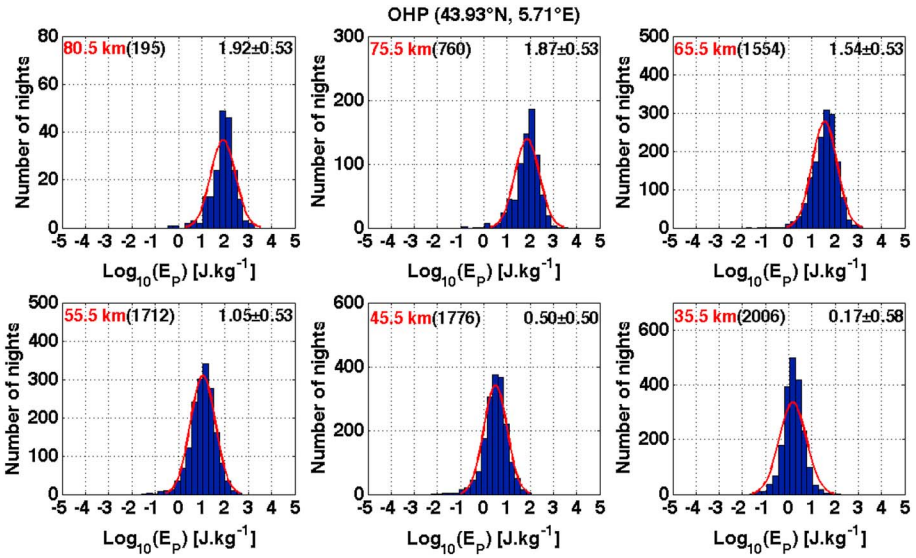


**Figure 3.** Histograms of the nightly distributions of the logarithm of potential energy per unit mass (in J.kg$^{-1}$) in the upper stratosphere and mesosphere from January 1996 to December 2012 derived from Rayleigh lidar over OHP (43.93°N, 5.71°E). Nightly $E_p$s are represented at several altitudes in the mesosphere (55.5, 65.5, 75.5, and 80.5 km) and upper stratosphere (35.5 and 45.5 km). The red line indicates the fit of the Gaussian normal distribution to the data. The number of profiles per altitude is also shown in the upper left corner of the axes. The mean and ±1σ standard deviation are represented in the upper right corner of the axes.

Figure 5 shows the contour plots of the gravity wave potential energy climatology from lidar observations. $E_p$ is colored in a logarithmic scale (log10). As expected, we find an annual cycle with a maximum of gravity wave activity occurring in winter and a minimum in summer in the upper stratosphere. The gravity wave activity is larger during winter than during summer in the 30–50 km altitude range. An annual cycle is also observed with maximum in winter and minimum during summer in the lower mesosphere (50–60 km). We found a semiannual cycle with maxima of gravity wave potential energy occurring in winter and in summer and

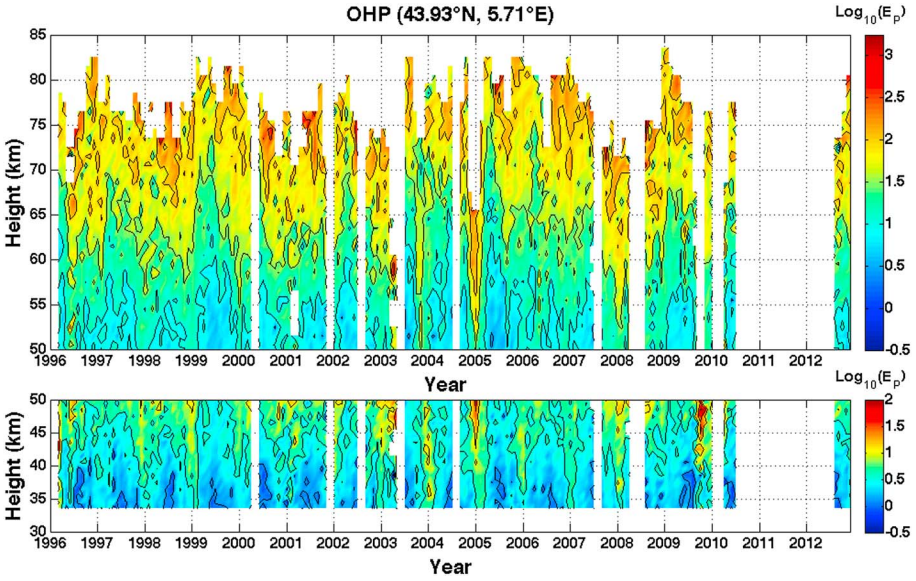


**Figure 4.** Monthly median distributions of potential energy per unit mass (in J.kg$^{-1}$) as derived from lidar measurements. $E_p$ is colored in a logarithmic scale (log10). The contours are separated by 0.5 J.kg$^{-1}$. The three-point variance is computed with two different values of $N_z$ in two layers, i.e., with $\Delta Z$ ranging from 1.5 km ($N_z = 20$) in (bottom) the upper stratosphere (30–50 km) to 3 km ($N_z = 40$) in (top) the mesosphere (50–85 km).

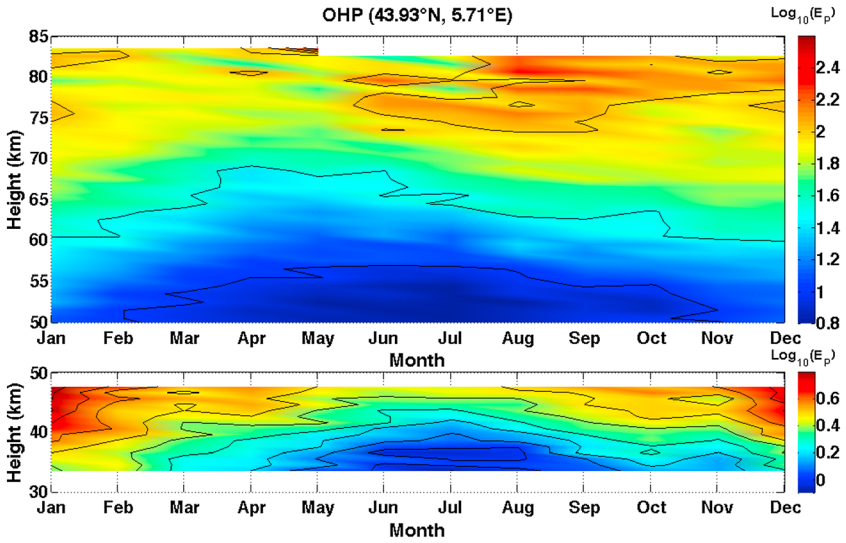


**Figure 5.** Contour plots of the gravity wave potential energy climatology (in J.kg$^{-1}$) from lidar observations. $E_p$ is colored in a logarithmic scale (log10). The contours are separated by 0.2 J kg$^{-1}$.

minima occurring during the equinoxes in the upper mesosphere. A secondary maximum of the gravity wave activity occurs in summer (June, July, and August) at ~75 km.

Figure 6 presents the average annual cycle of the gravity wave potential energy as derived from lidar observations. As mentioned above, we found an annual cycle with a maximum of gravity wave activity occurring in winter and a minimum in summer in the upper stratosphere and lower mesosphere (e.g., 45.5 and 55.5 km). The amplitude of the seasonal variation in the upper stratosphere (a factor ranging between 2.4 and 3.6) is quite similar in the lower mesosphere (a factor ranging between 2.2 and 3.4). We found a semiannual cycle with maxima of gravity wave potential energy occurring in winter and in summer and minima occurring during the equinoxes in the upper mesosphere (e.g., 75.5 km). At 75.5 km, in August, the $E_p$ is a factor of 2.5 larger than in April, and it is a factor of 2 larger than in October. In January, the $E_p$ is a factor of 2 larger than in April. The secondary maximum in summer (144 J kg$^{-1}$ on average in August) seems slightly stronger and more pronounced than the winter maximum (115 J kg$^{-1}$ on average in January).

## 5. Seasonal Changes and Energy Dissipation as a Function of Altitude

Seasonal averages of gravity wave potential energy based on lidar observations over the 16 year time period are illustrated in Figure 7. Vertical profiles have been averaged over winter (December-January-February, 519 profiles), spring (March-April-May, 475 profiles), summer (June-July-August, 531 profiles), and autumn (September-October-November, 554 profiles). If the seasonal profile of gravity wave $E_p$ is constant with height, this indicates undamped wave propagation. The conservative growth curve is superimposed. In the upper stratosphere and middle mesosphere (30–70 km), $E_p$ values in winter are larger than in summer as expected. The values in spring and autumn are quite similar in the upper stratosphere. In the upper mesosphere, winter values are lower than summer values. It can be observed from Figure 7 that the vertical growth of $E_p$ seems to follow the conservative growth curve in the upper stratosphere. We observed that $E_p$ is increasing with altitude at a slower rate than in the midstratosphere from ~45 km to the lower mesosphere (~55 km) in all seasons. It could be linked to the stratopause layer, which could lead to filtering and dissipation as previously observed at middle latitudes [*Wilson et al*., 1991a; *Rauthe et al*., 2006]. *Rauthe et al*. [2006] suppose that changing the static stability causes the increased filtering and breaking in their observations. Then the vertical growth rate of $E_p$ has approximately the same gradient as the conservative growth rate up to ~70 km, but there seems to be some indication for dissipation also between ~60 and ~70 km altitudes. Above ~70 km, it is clear that $E_p$ values do not increase at the conservative growth rate, which indicates some loss of gravity wave energy and dissipation or saturation in the upper mesosphere.

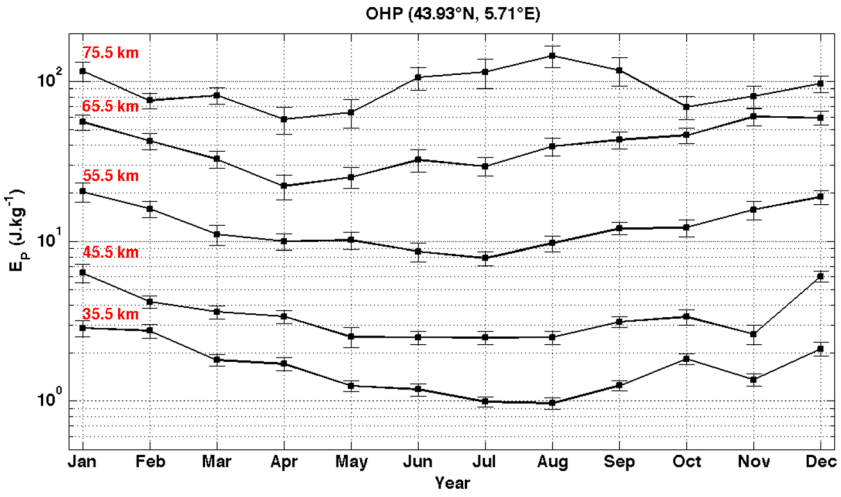


**Figure 6.** Average annual cycle of the gravity wave potential energy per unit mass (in J.kg$^{-1}$) over OHP. Averages are represented at several altitudes (10 km intervals) in the upper stratosphere (35.5 and 45.5 km) and in the mesosphere (55.5, 65.5, and 75.5 km). The vertical error bars indicate the ±1σ uncertainty of the median. Note the logarithmic scale of the *y* axis.

The potential energy per unit volume (in J.m$^{-3}$) as a function of altitude and season is depicted in Figure 8. It is obtained by multiplying the potential energy per unit mass by the density derived from the lidar measurements and for conserved gravity waves (propagating upward without energy dissipation), the energy per unit volume lines would be vertical (the values remain constant). We observed nonconservation of $E_p$ in the upper stratosphere/lower mesosphere (30–~55 km), so there is some wave dissipation. Then we observed approximate energy conservation up to ~70 km during summertime (note the vertical $E_p$, red line on Figure 8 in this region), but some wave dissipation in other seasons, especially in winter and spring. Above 70 km, waves are being dissipated in all seasons as evidenced by the large change in the vertical gradient of $E_p$ per unit volume. It indicates more dissipation and/or filtering of wave energy in the background atmosphere.

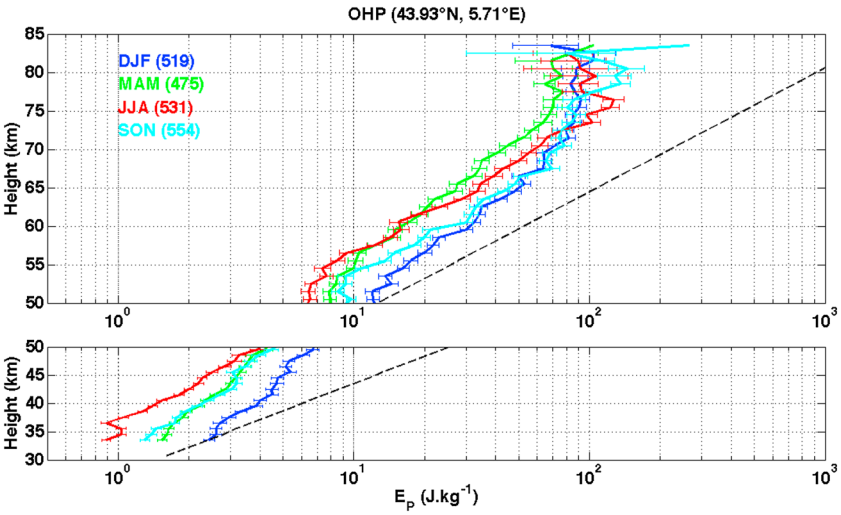


**Figure 7.** Vertical profiles of potential energy per unit mass (in J.kg$^{-1}$) in the upper stratosphere and mesosphere averaged over winter (December-January-February, blue line), spring (March-April-May, green line), summer (June-July-August, red line), and autumn (September-October-November, cyan line). The conservative growth curve is also superimposed (black dashed line) with a constant density scale height *H*~7 km. The horizontal error bars indicate the ±1σ uncertainty of the median. The number of profiles used for the seasonal average is represented in the upper left corner of the axes. Note the logarithmic scale of the *x* axis.

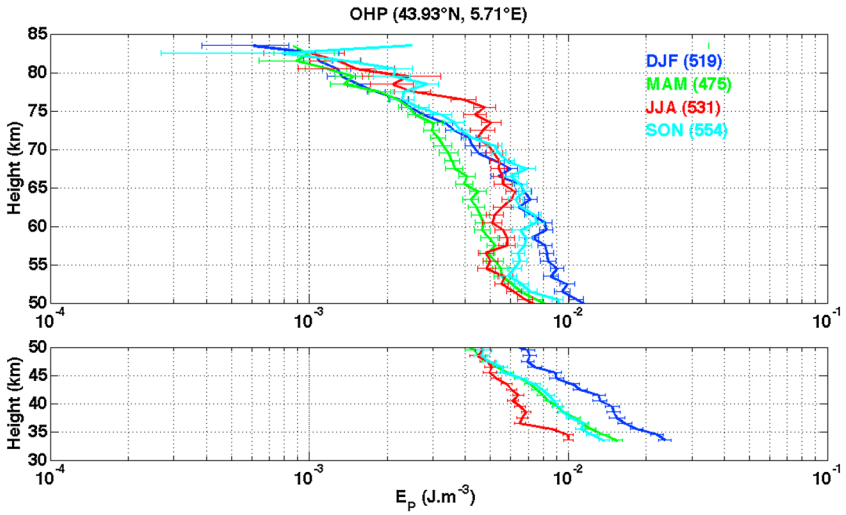


**Figure 8.** The same as Figure 7 except for the vertical profiles of potential energy per unit volume (in $J.m^{-3}$).

Thus, we observed damping of gravity waves in all seasons depending on the altitude. This damping is probably due to instabilities (convective or dynamical) or critical layer filtering. Our results are consistent with previous studies in the middle latitudes [*Gardner et al*., 1989; *Mitchell et al*., 1991; *Whiteway and Carswell*, 1995; *Rauthe et al*., 2008]. It is also interesting to note that our results are consistent with high-latitude studies, e.g., at Eureka, Arctic [*Whiteway and Carswell*, 1994], and above Davis, Antarctic [*Alexander et al*., 2011], with significant wave dissipation in the mesosphere (i.e., nonconstant $E_p$ per unit volume with altitude).

## 6. Discussion

We pointed out a night-to-night variability, an interannual variability, and an annual cycle of gravity wave activity with maximum in winter and minimum in summer in the upper stratosphere and lower mesosphere. These results correspond to those obtained with lidar measurements at different midlatitude stations [*McDonald et al*., 1998; *Mitchell et al*., 1991; *Murayama et al*., 1994; *Rauthe et al*., 2006, 2008; *Sica and Argall*, 2007; *Whiteway and Carswell*, 1995] and at OHP [*Wilson et al*., 1991b]. *Wilson et al*. [1991b] provided the gravity wave climatology above OHP using 3 years of lidar data from 1986 to 1989. They found that the maximum of wave activity occurs during winter and minimum during summer in the stratosphere and lower mesosphere. They also pointed out a day-to-day variability of the wave energy density and a significant positive correlation between the wave activity and the wind intensity in the stratosphere. Using observations made in 1990–1991 at Tsukuba (36°N, 140°E), *Murayama et al*. [1994] found an annual variation with a winter maximum in the upper stratosphere. *Whiteway and Carswell* [1995], using data from June 1991 to June 1992, obtained that gravity wave activity varied considerably from day to day and seasonally with a winter maximum and a summer minimum over Toronto (44°N, 80°W). Using the combined data set of two lidars (Rayleigh–Mie–Raman and potassium resonance lidar) from 2002 to 2006, *Rauthe et al*. [2006, 2008] reported a clear seasonal variation of the gravity wave activity with maximum in winter over Kühlungsborn (54°N, 12°E). A study performed by *Sica and Argall* [2007] from 1994 to 2004 (146 nights) provided a considerable day-to-day variability at Delaware Observatory (42.9°N, 81.4°W). *McDonald et al*. [1998] observed during periods of 4 days in February 1993 and in June 1995 night-to-night changes in wave activity using Rayleigh lidar observations at Aberystwyth (52.4°N, 4.1°W). *Mitchell et al*. [1991] found an annual cycle and a day-to-day variability at Aberystwyth using 50 nights from October 1987 to September 1990.

Different authors argued that the background temperature and density play a role to explain the observed annual variation, i.e., the winter-summer differences [e.g., *Rauthe et al*., 2006, 2008, and references therein]. *Wilson et al*. [1991b] and *Whiteway and Carswell* [1995] have discussed on the influence of the critical level filtering of gravity wave by the background wind [*Lindzen*, 1981]. Gravity wave encounters a critical layer when the horizontal phase speed of the wave equals the mean zonal wind speed. In their study, *Rauthe et al*. [2008] reported that no statement was possible yet due to their observations (different gravity wave sources

following the season; the gravity waves observed by a lidar are not necessarily influenced by the local wind field below because of the tilted propagation of the waves). They found no direct correlation between the strength of the gravity wave activity and the wind direction and/or wind speed.

We also pointed out a semiannual cycle at ~75 km with the maximum of gravity wave activity occurring in winter and in summer. This corresponds to the results of *Wilson et al*. [1991b]. They observed a semiannual variation above 60 km with a maximum in winter and in summer and minima in April–May and September (when the mean wind intensity is weak) at OHP. *Senft and Gardner* [1991] also reported a semiannual variation in the mesopause region from 60 nights of Na lidar measurements at Urbana (40°N, 88°W) over a 5 year period. This seasonal variation in gravity wave activity has also been reported at middle-latitude sites in the ~65–90 km altitude range using radar observations [e.g., *Fritts and Alexander*, 2003, and references therein]. The authors reported a semiannual variation with maxima in summer and winter and minima in spring and fall. Recently, *Hoffmann et al*. [2010] investigated seasonal variations of gravity wave in the mesosphere/lower thermosphere using wind measurements with the MF radar at Juliusruh (55°N, 13°E). They reported a semiannual variation with maxima during winter and summer and minima during the equinoxes. It is assumed that the filtering of gravity wave by the background wind in the stratosphere and lower mesosphere is the main factor determining this seasonal dependence. They added that the absolute minima around the equinoxes are probably due to the very weak zonal wind, which favors the damping of both eastward and westward propagating gravity waves.

The local data set is also in agreement with the global picture as seen from satellite data over midlatitudes [e.g., *Preusse et al*., 2009; *Gong et al*., 2012; *John and Kumar*, 2012]. This is not trivial, since different measurements have different methods to remove the large-scale background and have different observational filters. For instance, *Preusse et al*. [2009] show the same change in the annual cycle we observe: a winter maximum in the stratosphere and a semiannual variation of gravity wave variances in the mesosphere and mesosphere lower thermosphere, with the summer maximum becoming increasingly more important at higher altitudes. They reproduce this behavior by global ray-tracing simulations. These simulations show that filtering and modulation by the background wind (together with source variations) is the dominant influence to generate these patterns. Considering global distributions of absolute values of gravity wave momentum flux, *Ern et al*. [2011] show that in summer, gravity waves from subtropical convective sources propagate poleward and avoid in this way the summer wind reversal between troposphere and stratosphere. Around ~75 km altitude, these subtropical waves spread to 45°N, and the summertime maximum becomes important. For altitudes in the mesosphere lower thermosphere, however, very fast waves are dominant according to ray-tracing simulations [*Preusse et al*., 2009]. These waves have phase speeds sufficiently fast not to be filtered by the wind reversal at the tropopause. In order to shed light on the relative importance of poleward propagating gravity waves from the subtropics and fast gravity waves, comparisons to other stations farther northward is of interest. For instance, *Rauthe et al*. [2008] find at 54°N (Kühlungsborn) no indication for a summer maximum in the midmesosphere consistent with the global observations. This is evidence that oblique propagation causes the summer maximum at OHP in the midmesosphere.

Our data set complements the current state of knowledge on gravity waves. The annual cycle of gravity wave activity at the northern midlatitudes is already well documented as we have referenced; our results contribute to confirm these previous observations. We provide additional information on the vertical structure and on the interactions of the gravity waves and the mean flow with longer data basis, covering a larger altitude range over the *Wilson et al*.'s [1991b] results. Gravity wave energy dissipates in the background atmosphere depending on the altitude and the season above OHP. Gravity waves are dissipating above ~70 km during all seasons, but there is relatively little dissipation at lower altitudes.

## 7. Conclusions

This study concentrates on gravity wave activity in the upper stratosphere and mesosphere over OHP. These results demonstrate the ability of the lidar instrument to extract gravity wave potential energy throughout the middle atmosphere using a variance method on the raw signal. We observed night-to-night variations in the lidar measurements, and we observed interannual variability in gravity wave activity. We also provided gravity wave climatology based on 16 years of Rayleigh lidar data in the middle atmosphere (30–85 km). This long time period provided information on seasonal patterns and variability. We clearly found an annual

**Table A1.** Characteristics of the Distribution of $S'$, $S'^2$, and $V_{obs}$[a]

| Variable | Mean | Standard Deviation | Type of Distribution |
|---|---|---|---|
| $S'$ | 0 | $\sqrt{\frac{3}{2\bar{S}}}$ | Nearly normal |
| $S'^2$ | $\frac{3}{2\bar{S}}$ | $\frac{3}{\sqrt{2\bar{S}}}$ | Gamma |
| $V_{obs}$ | $\frac{3}{2\bar{S}}$ | $\frac{3}{\sqrt{2N_{int}\bar{S}}}$ | Nearly normal |

[a]The 95.4% confidence interval, corresponding to 2σ, on $V_{obs}$ is $6/\sqrt{2N_{int}\bar{S}}$.

cycle with maximum in winter and minimum in summer in the upper stratosphere and lower mesosphere. We found a semiannual cycle at ~75 km in the upper mesosphere with maximum of gravity wave activity occurring in winter and in summer. A more pronounced summer maximum is observed (+25%). The summer maximum at OHP in the upper mesosphere is probably due to oblique propagation. Our findings agree with those obtained previously by lidars at northern midlatitude stations. Finally, we analyzed the seasonal variations in gravity wave activity, and we observed dissipation of gravity waves in all seasons. We observed more dissipation of gravity waves above ~70 km during all seasons, but there is relatively little dissipation at lower altitudes.

This analysis could be extended back to August 1978 in a future work in order to perform long-term trends. We intend also to separate between short-period and long-period gravity waves. In the stratosphere, the potential energy is dominated by long-period inertia-gravity waves. However, the vertical propagation of short-period gravity waves is more efficient. Another application could be the detection of short-scale perturbations in winds induced by gravity waves using Doppler lidar data at OHP.

Further studies are needed to investigate our long-term gravity wave activity and its connection with winds over OHP, to explain the observed inter-annual variability, and to better understand the gravity wave perturbations related to atmospheric events as sudden stratospheric warming over OHP. Lidar could provide long-term and high-resolution observations, which would help to study atmospheric dynamics and to improve weather and climate models.

## Appendix A

As mentioned in the main text, the estimation of the atmospheric variance is obtained by difference:

$$V_{atm} = V_{obs} - V_{inst} \tag{A1}$$

If the signal $S(z_i, t_j)$ is varying weakly around its mean value $\bar{S}$, the expression of the estimation of the instrumental variance may be simplified:

$$V_{inst} = \frac{3}{2\bar{S}} \tag{A2}$$

When doing such analysis, we want to determine if the estimated atmospheric variance is meaningfully above 0, which is equivalent to determine if $V_{obs}$ is meaningfully different from $V_{inst}$. In order to do that, we first estimate the standard deviation of $V_{obs}$ in the case where perturbations are only due to instrumental noise. As soon as the mean signal $\bar{S}$ is large enough (more than about 100 counts per elementary interval), we can apply the central limit theorem [*Kreyszig*, 1988], and the perturbation $S'(z_i, t_j)$ converges toward a Gaussian distribution with mean equal to 0 and standard deviation equal to $\sqrt{3/2\bar{S}}$. Following *Dwass* [1970], the square of a normal distribution with mean 0 and variance standard deviation $\sigma^2$ of the form

$$f(x) = \frac{1}{\sigma\sqrt{2\pi}} e^{-\frac{x^2}{2\sigma^2}} \tag{A3}$$

is a gamma distribution of the form

$$g(y) = \frac{1}{\sqrt{\pi}} y^{-\frac{1}{2}} e^{-y} \tag{A4}$$

with $y = x^2/2\sigma^2$.

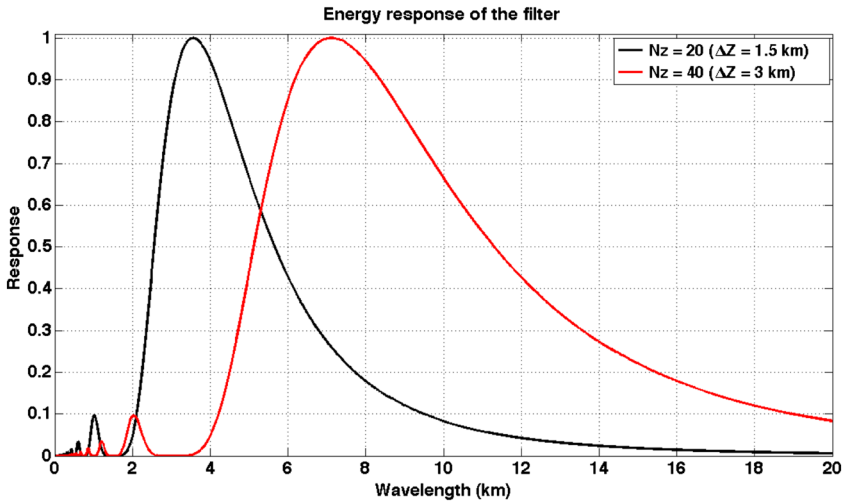


**Figure B1.** Passbands in the energy of the filter used in the estimation of the variance for $N_z = 20$ (black line) and $N_z = 40$ (red line).

The expected mean value and variance of $y$ are 0.5. The expected mean value and standard deviation of $x^2$ are, respectively, $\sigma^2$ and $\sqrt{2}\sigma^2$. This result can be applied to the square of the perturbation $S'(z_i, t_j)^2$. Its distribution is of course not normal, but its average $V_{obs}$ has a nearly normal distribution as soon as the number of elementary intervals $N_{int}$ is large enough (applying again the central limit theorem). Table A1 summarizes these results.

With these hypotheses, it is possible to determine the number of elementary interval necessary to detect a given atmospheric perturbation of a relative root-mean-square amplitude $\delta$:

$$N_{int} = \frac{18}{\delta^4 \overline{S}^2} \tag{A5}$$

This estimation does not take into account the overlapping in altitude of consecutive elements $S'(z_i, t_j)$ that will increase $N_{int}$ but will not change the dependence in $\delta$ and $\overline{S}$. This formula shows that it is possible to decrease the detectivity threshold of the perturbations by increasing the number of elementary intervals over which the average is made. It shows also the great sensitivity of $N_{int}$ to the mean signal (inverse of its square) and to the amplitude of perturbations (inverse of its fourth power).

## Appendix B: Spectral Analysis

In the case of the linear formula with a constant signal $\overline{S}$ plus small-amplitude perturbations, it is possible to analytically compute the response of the filter. In this case, the denominator of equation (2) is equal to $\overline{S}$ and the numerator can be decomposed in a sum of $n$ integrals of the signal in square windows of width $k\Delta Z$ with $k$ equals 1 to $n$. The Fourier transform of the square window of width $k\Delta Z$ centered at 0 is

$$F(m) = \frac{\sin(k\Delta Z m/2)}{m} \tag{B1}$$

where $m$ is the vertical wave number.

The response of the filter energy (square of the amplitude of the Fourier transform) has been computed for the three-point filter. The passband of this filter is represented in Figure B1 for $\Delta Z = 1.5$ km ($N_z = 20$) and for

**Table B1.** Characteristics of Three-Points Filter

| | | | $\Delta\lambda/\Delta Z$ |
|---|---|---|---|
| $N$ points | Normalization Coefficient | $\lambda_{max}/\Delta Z$ | ($\Delta\lambda$ at Half Response) |
| 3 | 0.527 | 2.37 | 2.06 |

**Table B2.** Characteristics of the Vertical Filter

| Altitude Range (km) | $\Delta Z$ (km) |
|---|---|
| 30–50 | 1.5 |
| 50–85 | 3 |

$\Delta Z = 3$ km ($N_z = 40$). It is unphysical to have response greater than 1, which was the case using the coefficients obtained from equation (2), and the response has been normalized to 1 at the frequency of the maximum of response, and normalization coefficient is given in Table B1. Variances presented in the present study are then normalized with this coefficient in order to have a maximum response of the filter of 1 (see also an example given by *Hauchecorne et al.* [1994] in their Figure 2). The three-point variance has been computed in two layers with $\Delta T = 26$ min and $\Delta Z$ ranging from 1.5 km in the upper stratosphere (30–50 km) to 3 km in the mesosphere (50–85 km) as indicated in Table B2. The three-point variance is already a good estimator of the energy in a broad band ($\Delta m \approx m$) centered at a wavelength $\lambda$ slightly greater than $2\Delta Z$.

**Acknowledgments**

This work has been made in the frame of the FP7 EU project ARISE (Atmospheric dynamics Research InfraStructure in Europe) and the ANR project Stratospheric Dynamics and Variability: Understanding and Solutions to persistent model biases. Lidar measurements at Haute-Provence Observatory were obtained in the frame of the NDACC (Network for the Detection of Atmospheric Composition Changes) with the support of Centre National de la Recherche Scientifique—Institut des Sciences de l'Univers, Centre National d'Etudes Spatiales, and Université de Versailles Saint-Quentin-en-Yvelines. NDACC data are publicly available on the NOAA database (http://www.ndsc.ncep.noaa.gov). Data and plots can also be found through the French Data Center ETHER (http://www.pole-ether.fr). Gravity wave product will be available on the ETHER database and on the ARISE portal. To process the variance estimates as performed and reported in this manuscript, raw lidar data are required and can only be available on request to authors. Finally, we thank the Editor and three anonymous reviewers for their valuable comments on the original manuscript.

## References

Alexander, M. J., et al. (2010), Recent developments in gavity-wave effects in climate models and the global distribution of gravity-wave momentum flux from observations and models, *Q. J. R. Meteorol. Soc.*, *136*, 1103–1124, doi:10.1002/qj.637.

Alexander, S. P., A. R. Klekociuk, and D. J. Murphy (2011), Rayleigh lidar observations of gravity wave activity in the winter upper stratosphere and lower mesosphere above Davis, Antarctica (69°S, 78°E), *J. Geophys. Res.*, *116*, D13109, doi:10.1029/2010JD015164.

Beatty, T. J., C. A. Hostetler, and C. S. Gardner (1992), Lidar observations of gravity waves and their spectra near the Mesopause and Stratopause at Arecibo, *J. Atmos. Sci.*, *49*, 477–496.

Blum, U., K. H. Fricke, G. Baumgarten, and A. Schöch (2004), Simultaneous lidar observations of temperatures and waves in the polar middle atmosphere on the east and west side of the Scandinavian mountains: A case study on 19/20 January 2003, *Atmos. Chem. Phys.*, *4*, 809–816, doi:10.5194/acp-4-809-2004.

Chane-Ming, F., F. Molinaro, J. Leveau, P. Keckhut, and A. Hauchecorne (2000), Analysis of gravity waves in the tropical middle atmosphere over La Reunion Island (21°S, 55°E) with lidar using wavelet techniques, *Ann. Geophys.*, *18*, 485–498, doi:10.1007/s00585-000-0485-0.

Chanin, M.-L., and A. Hauchecorne (1981), Lidar observations of gravity and tidal waves in the stratosphere and mesosphere, *J. Geophys. Res.*, *86*(C10), 9715–9721, doi:10.1029/JC086iC10p09715.

Collins, R. L., A. Nomura, and C. S. Gardner (1994), Gravity waves in the upper mesosphere over Antarctica: Lidar observations at the South Pole and Syowa, *J. Geophys. Res.*, *99*(D3), 5475–5485, doi:10.1029/93JD03276.

Duck, T. J., J. A. Whiteway, and A. I. Carswell (2001), The gravity wave-arctic stratospheric vortex interaction, *J. Atmos. Sci.*, *58*(23), 3581–3596, doi:10.1175/1520-0469(2001)058<3581:TGWASV>2.0.CO;2.

Dwass, M. (1970), *Probability and Statistics: An Undergraduate Course*, W.A. Benjamin, New York.

Ern, M., P. Preusse, J. C. Gille, C. L. Hepplewhite, M. G. Mlynczak, J. M. Russell, and M. Riese (2011), Implications for atmospheric dynamics derived from global observations of gravity wave momentum flux in stratosphere and mesosphere, *J. Geophys. Res.*, *116*, D19107, doi:10.1029/2011JD015821.

Fritts, D. C., and M. J. Alexander (2003), Gravity wave dynamics and effects in the middle atmosphere, *Rev. Geophys.*, *41*(1), 1003, doi:10.1029/2001RG000106.

Gardner, C. S., and D. G. Voelz (1987), Lidar studies of the nighttime sodium layer over Urbana, Illinois: 2. Gravity waves, *J. Geophys. Res.*, *92*(A5), 4673–4694, doi:10.1029/JA092iA05p04673.

Gardner, C. S., M. S. Miller, and C. H. Liu (1989), Rayleigh lidar observations of gravity wave activity in the upper stratosphere at Urbana, Illinois, *J. Atmos. Sci.*, *46*(12), 1838–1854, doi:10.1175/1520-0469(1989)046<1838:RLOOGW>2.0.CO;2.

Geller, M. A., et al. (2013), A comparison between gravity wave momentum fluxes in observations and climate models, *J. Clim.*, *26*, 6383–6405, doi:10.1175/JCLI-D-12-00545.1.

Gong, J., D. L. Wu, and S. D. Eckermann (2012), Gravity wave variances and propagation derived from AIRS radiances, *Atmos. Chem. Phys.*, *12*, 1701–1720, doi:10.5194/acp-12-1701-2012.

Hauchecorne, A., and M. L. Chanin (1980), Density and temperature profiles obtained by lidar between 35 and 70 km, *Geophys. Res. Lett.*, *7*(8), 565–568, doi:10.1029/GL007i008p00565.

Hauchecorne, A., and A. Maillard (1990), A 2-d dynamical model of mesospheric temperature inversions in winter, *Geophys. Res. Lett.*, *17*(12), 2197–2200, doi:10.1029/GL017i012p02197.

Hauchecorne, A., M. L. Chanin, and R. Wilson (1987), Mesospheric temperature inversion and gravity wave breaking, *Geophys. Res. Lett.*, *14*(9), 933–936, doi:10.1029/GL014i009p00933.

Hauchecorne, A., M. L. Chanin, and P. Keckhut (1991), Climatology and trends of the middle atmospheric temperature (33–87 km) as seen by Rayleigh lidar over the south of France, *J. Geophys. Res.*, *96*(D8), 15,297–15,309, doi:10.1029/91JD01213.

Hauchecorne, A., M. L. Chanin, P. Keckhut, and D. Nedeljkovic (1992), LIDAR monitoring of the temperature in the middle and lower atmosphere, *Appl. Phys. B*, *55*(1), 29–34.

Hauchecorne, A., et al. (1994), Gravity-wave activity and its relation with prevailing winds during DYANA, *J. Atmos. Terr. Phys.*, *56*(13), 1765–1778.

Hauchecorne, A., P. Keckhut, and M. L. Chanin (2009), Dynamics and transport in the middle atmosphere using remote sensing techniques from ground and space, in *Infrasound Monitoring for Atmospheric Studies*, edited by A. Le Pichon, E. Blanc, and A. Hauchecorne, pp. 665–683, Springer, Netherlands, doi:10.1007/978-1-4020-9508-5_22.

Hoffmann, P., E. Becker, W. Singer, and M. Placke (2010), Seasonal variation of mesospheric waves at northern middle and high latitudes, *J. Atmos. Sol. Terr. Phys.*, *72*(14–15), 1068–1079, doi:10.1016/j.jastp.2010.07.002.

John, S. R., and K. K. Kumar (2012), TIMED/SABER observations of global gravity wave climatology and their interannual variability from stratosphere to mesosphere lower thermosphere, *Clim. Dyn.*, *39*, 1489–1505, doi:10.1007/s00382-012-1329-9.

Keckhut, P., A. Hauchecorne, and M. L. Chanin (1993), A critical review of the database acquired for the long-term surveillance of the middle atmosphere by the French Rayleigh lidars, *J. Atmos. Oceanic Tech.*, *10*, 850–867.

Kim, Y.-J., S. D. Eckermann, and H.-Y. Chun (2003), An overview of the past, present and future of gravity•wave drag parameterization for numerical climate and weather prediction models, *Atmos. Ocean*, *41*, 65–98, doi:10.3137/ao.410105.

Kreyszig, E. (1988), *Advanced Engineering Mathematics*, John Wiley, New York.

Li, T., T. Leblanc, I. S. McDermid, D. L. Wu, X. Dou, and S. Wang (2010), Seasonal and interannual variability of gravity wave activity revealed by long-term lidar observations over Mauna Loa Observatory, Hawaii, *J. Geophys. Res.*, *115*, D13103, doi:10.1029/2009JD013586.

Lindzen, R. S. (1981), Turbulence and stress owing to gravity wave and tidal breakdown, *J. Geophys. Res.*, *86*(C10), 9707–9714, doi:10.1029/JC086iC10p09707.

McDonald, A. J., L. Thomas, and D. F. Wareing (1998), Night-to-night changes in the characteristics of gravity waves at stratospheric and lower-mesospheric heights, *Ann. Geophys.*, *16*, 229–237.

Meriwether, J. W., and C. S. Gardner (2000), A review of the mesosphere inversion layer phenomenon, *J. Geophys. Res.*, *105*(D10), 12,405–12,416, doi:10.1029/2000JD900163.

Mitchell, N. J., L. Thomas, and A. K. P. Marsh (1991), Lidar observations of long-period gravity waves in the stratosphere, *Ann. Geophys.*, *9*, 588–596.

Murayama, Y., T. Tsuda, R. Wilson, H. Nakane, S. A. Hayashida, N. Sugimoto, I. Matsui, and Y. Sasano (1994), Gravity wave activity in the upper stratosphere and lower mesosphere observed with the Rayleigh lidar at Tsukuba, Japan, *Geophys. Res. Lett.*, *21*(14), 1539–1542, doi:10.1029/93GL02693.

Preusse, P., S. D. Eckermann, M. Ern, J. Oberheide, R. H. Picard, R. G. Roble, M. Riese, J. M. Russell, and M. G. Mlynczak (2009), Global ray tracing simulations of the SABER gravity wave climatology, *J. Geophys. Res.*, *114*, D08126, doi:10.1029/2008JD011214.

Rauthe, M., M. Gerding, J. Höffner, and F.-J. Lübken (2006), Lidar temperature measurements of gravity waves over Kühlungsborn (54°N) from 1 to 105 km: A winter-summer comparison, *J. Geophys. Res.*, *111*, D24108, doi:10.1029/2006JD007354.

Rauthe, M., M. Gerding, and F.-J. Lübken (2008), Seasonal changes in gravity wave activity measured by lidars at mid-latitudes, *Atmos. Chem. Phys.*, *8*, 6775–6787, doi:10.5194/acp-8-6775-2008.

Ridolfi, M., et al. (2007), Geophysical validation of temperature retrieved by the ESA processor from MIPAS/ENVISAT atmospheric limb-emission measurements, *Atmos. Chem. Phys.*, *7*, 4459–4487, doi:10.5194/acp-7-4459-2007.

Senft, D. C., and C. S. Gardner (1991), Seasonal variability of gravity wave activity and spectra in the mesosphere region at Urbana, *J. Geophys. Res.*, *96*, 17, 229–17, 264, doi:10.1029/91JD01662.

Shibata, T., M. Kobuchi, and M. Maeda (1986), Measurements of density and temperature profiles in the middle atmosphere with a XeF lidar, *Appl. Opt.*, *25*(5), 685–688.

Sica, R. J., and P. S. Argall (2007), Seasonal and nightly variations of gravity-wave energy density in the middle atmosphere measured by the Purple Crow Lidar, *Ann. Geophys.*, *25*, 2139–2145, doi:10.5194/angeo-25-2139-2007.

Sica, R. J., et al. (2008), Validation results for the Atmospheric Chemistry Experiment (ACE), *Atmos. Chem. Phys.*, *8*, 35–62, doi:10.5194/acp-8-35-2008.

Singh, U. N., P. Keckhut, T. J. McGee, M. R. Gross, A. Hauchecorne, E. F. Fishbein, J. W. Waters, J. C. Gille, A. E. Roche, and J. M. Russell III (1996), Stratospheric temperature measurements by two collocated NDSC lidars at OHP during UARS validation campaign, *J. Geophys. Res.*, *101*(D6), 10,287–10,297, doi:10.1029/96JD00516.

Sivakumar, V., P. B. Rao, and H. Bencherif (2006), Lidar observations of middle atmospheric gravity wave activity over a low-latitude site (Gadanki, 13.5°N, 79.2°E), *Ann. Geophys.*, *24*, 823–834, doi:10.5194/angeo-24-823-2006.

Steinbrecht, W., et al. (2009), Ozone and temperature trends in the upper stratosphere at five stations of the network for the detection of atmospheric composition change, *Int. J. Remote Sens.*, *30*, 3875–3886.

Warner, C. D., and M. E. McIntyre (1999), Toward an ultra-simple spectral gravity wave parameterization for general circulation models, *Earth Planets Space*, *51*, 475–484.

Whiteway, J. A., and A. I. Carswell (1994), Rayleigh lidar observations of thermal structure and gravity wave activity in the high Arctic during a stratospheric warming, *J. Atmos. Sci.*, *51*, 3122–3136.

Whiteway, J. A., and A. I. Carswell (1995), Lidar observations of gravity wave activity in the upper stratosphere over Toronto, *J. Geophys. Res.*, *100*, 14,113–14,124, doi:10.1029/95JD00511.

Whiteway, J. A., T. J. Duck, D. P. Donovan, J. C. Bird, S. R. Pal, and A. I. Carswell (1997), Measurements of gravity wave activity within and around the arctic stratospheric vortex, *Geophys. Res. Lett.*, *24*, 1387–1390, doi:10.1029/97GL01322.

Wilson, R., A. Hauchecorne, and M. L. Chanin (1990), Gravity wave spectra in the middle atmosphere as observed by Rayleigh lidar, *Geophys. Res. Lett.*, *17*(10), 1585–1588, doi:10.1029/GL017i010p01585.

Wilson, R., M. L. Chanin, and A. Hauchecorne (1991a), Gravity waves in the middle atmosphere observed by Rayleigh lidar: 1. Case studies, *J. Geophys. Res.*, *96*(D3), 5153–5167, doi:10.1029/90JD02231.

Wilson, R., M. L. Chanin, and A. Hauchecorne (1991b), Gravity waves in the middle atmosphere observed by Rayleigh lidar: 2. Climatology, *J. Geophys. Res.*, *96*(D3), 5169–5183, doi:10.1029/90JD02610.

Yamashita, C., X. Chu, H.-L. Liu, P. J. Espy, G. J. Nott, and W. Huang (2009), Stratospheric gravity wave characteristics and seasonal variations observed by lidar at the South Pole and Rothera, Antarctica, *J. Geophys. Res.*, *114*, D12101, doi:10.1029/2008JD011472.